

Application of the multi-scale enveloping spectrogram to detect weak faults in a wind turbine gearbox

ISSN 1752-1416
 Received on 15th August 2016
 Revised 9th January 2017
 Accepted on 18th January 2017
 E-First on 10th February 2017
 doi: 10.1049/iet-rpg.2016.0722
 www.ietdl.org

Zhiyong Ma¹, Wei Teng^{1,2} ✉, Yibing Liu^{1,2}, Dameng Wang¹, Andrew Kusiak³

¹School of Energy, Power and Mechanical Engineering, North China Electric Power University, Beijing 102206, People's Republic of China

²Key Laboratory of Condition Monitoring and Control for Power Plant Equipment of Ministry of Education, North China Electric Power University, Beijing 102206, People's Republic of China

³Mechanical and Industrial Engineering, 3131 Seamans Center, The University of Iowa, Iowa City, IA 52242-1527, USA

✉ E-mail: tengw@ncepu.edu.cn

Abstract: The gearbox of a wind turbine involves multiple rotating components, each having a potential to be affected by a fault. Detecting weak faults of these components with traditional demodulation analysis is challenging. Multi-scale enveloping spectrogram (MuSEnS) decomposes a vibration signal into different frequency bands while simultaneously generating the corresponding envelope spectra. In this study, a MuSEnS-based diagnosis approach is applied to detect faults affecting the intermediate stage of a gearbox installed in an operating wind turbine. The MuSEnSs of 12 vibration channels have allowed to identify multiple fault features, including the weak fault of the big gear on the sun shaft. The effectiveness of the proposed fault diagnosis approach has been tested with industrial data and the faults themselves have been confirmed with the disassembled gears.

1 Introduction

Wind energy is the fastest growing form of renewable energy generation combatting greenhouse effects. The harsh operating environment of wind turbines contributes failures of their assemblies, components and systems. The wind turbine gearbox that bears alternating loads, it is one of the most affected parts in wind turbine [1, 2].

Once fault arises in the wind turbine gearbox, it is inevitable that the power generation efficiency is reduced, and eventually an unscheduled downtime occurs. Condition monitoring and fault diagnosis (CMFD) systems are intended to detect conditions leading to faults of a gearbox and recommend timely maintenance [3, 4]. Amirata *et al.* [5] discussed the importance of CMFD in blades, gearbox, and generator, and described different types of faults, their signatures, and recommended diagnostic schemes. Wymore [6] surveyed the commercially available products for health monitoring of wind turbines, and quantified the cost saved by each turbine due to continuous monitoring. Tchakoua *et al.* [7] reviewed the related techniques of condition monitoring, fault diagnosis, and maintenance analysis, and predicted that intelligent health management will be the trend of the CMFD of wind turbines. Without doubt, intelligent health management needs the support of advanced approaches of fault diagnosis for wind turbines.

In terms of diagnosis methods, Yang *et al.* [8] utilised a wavelet transform to detect fault in the drive train of a test rig with the current and power signals. Zhang *et al.* [9] applied data mining algorithms and statistical methods to analyse the derivative of vibration signals and considered the correlation coefficient in identification of a gear fault. Feng and Zuo [10] proposed torsional vibration model to detect distributed and local defects in a planetary gearbox providing a theoretical foundation of fault diagnosis in wind turbine gearboxes. Lapira *et al.* [11] proposed a multi-regime modelling approach to assess the degradation of wind turbine before downtime occurrences using supervisory control and data acquisition data. Herp *et al.* [12] used Bayesian classifiers and multivariate analysis monitor the performance of wind turbines, and introduced a classification of turbines' faulty and normal state based on skewness and kurtosis.

Vibration analysis is a common method to monitor health conditions of gears and bearings in gearboxes. Although it calls for the installation of acceleration transducers on the surface of a gearbox, it offers high sensitivity of recognition of fault features and fault discovery. Lei *et al.* [13] utilised an ant colony algorithm to form adaptive stochastic resonance method, and detect a chipped tooth in the sun gear of planetary gearbox. Li *et al.* [14] adopted the denoising capability and high signal-to-noise ratio of a second-order enhanced stochastic resonance model to enhance the weak features and found looseness in a coupling between the gearbox and the generator. Teng *et al.* [15] detected multi-harmonic components representing gear pitting faults with empirical mode decomposition. Sun *et al.* [16] proposed a multiwavelet denoising technique with a data-driven block threshold to detect incipient fault of a bearing in wind turbines. Barszcz and Randall [17] applied spectral kurtosis to detect a tooth crack of a ring gear in the gearbox of an operating wind turbine. Feng *et al.* [18] established a fault model for a planetary transmission, and proposed different signal processing methods to detect gear faults with the ensemble empirical mode decomposition [19], iterative generalised synchrosqueezing transform [20], and adaptive optimal kernel time-frequency analysis [21].

The above discussed literature offers valuable research approaches to monitor and diagnose planetary gearboxes. However, some details of the gearboxes installed in industrial wind turbines have been overlooked, including multiple fault sources and a wide frequency range. In the gearbox of a 1.5 MW wind turbine, the rotational frequency of rotor hub is low (about 0.2 Hz), while the mesh frequency at the high speed stage (HSS) is about 700 Hz. These require high frequency resolution and wide frequency band to process vibration signal. Moreover, vibration energy at low or middle speed stage is likely masked by the mesh at HSS, which makes fault discovery at the low speed stage challenging.

In this paper, a multi-scale enveloping spectrogram (MuSEnS)-based fault diagnosis approach is proposed to detect faults in a wind turbine gearbox. Section 2 presents the structure of a wind turbine gearbox. The transmission ratio and feature frequencies are also calculated. The details of MuSEnS are outlined and the diagnosis procedure for wind turbine gearbox is proposed in

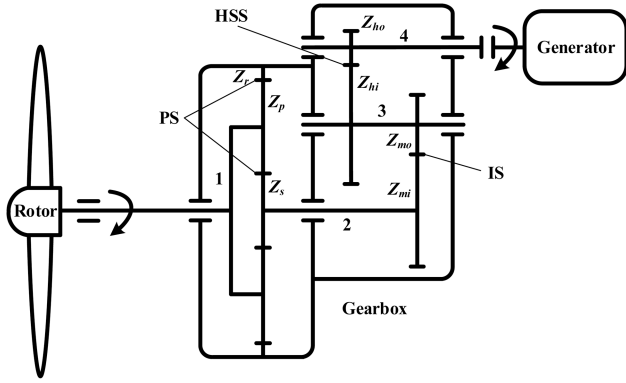


Fig. 1 Structure of a wind turbine gearbox

Section 3. In Section 4, the gearbox faults of an operating 2.0 MW wind turbine are analysed. The conclusion is drawn in Section 5.

2 Structure of a wind turbine gearbox

The rotor of a wind turbine converts the energy of the wind into a low speed mechanical energy which in turn is speeded up by the gearbox.

For compactness and high transmission ratio, a wind turbine gearbox consists of three stages: planetary stage (PS), intermediate stage (IS) and HSS. In the schematic diagram of the gearbox in Fig. 1, 1 is the planetary arm, 2 is the sun shaft, 3 is the intermediate shaft, and 4 is the high speed shaft. Sun gear Z_s , planetary gear Z_p , and ring gear Z_r make up PS; big gear Z_{mi} on the sun shaft and small gear Z_{mo} on the intermediate shaft mesh and form IS; big gear Z_{hi} on the intermediate shaft and gear Z_{ho} on the high speed shaft mesh and form HSS.

The transmission ratio of the PS is computed from the following equation.

$$r_{PS} = 1 + \frac{Z_r}{Z_s} \quad (1)$$

where Z_r is the number of teeth of ring gear, Z_s is the number of teeth of sun gear. The transmission ratio of IS is computed from the following equation.

$$r_{IS} = \frac{Z_{mi}}{Z_{mo}} \quad (2)$$

where Z_{mi} is the number of teeth of big gear on sun shaft, Z_{mo} is the number of teeth of the small gear on the intermediate shaft. The transmission ratio of HSS is computed according to the following equation.

$$r_{HSS} = \frac{Z_{hi}}{Z_{ho}} \quad (3)$$

where Z_{hi} is the number of teeth of the big gear on the intermediate shaft, Z_{ho} is the number of teeth of the gear on the high speed shaft. The total transmission ratio of gearbox is expressed as.

$$r = r_{PS} \cdot r_{IS} \cdot r_{HSS} \quad (4)$$

An emerging fault of a gear results in modulation of mesh frequency (natural frequency) by the rotational frequency of the shaft with the faulty gear. Therefore, it is necessary to compute the mesh frequencies of different stages and the rotational frequency of each shaft in the wind turbine gearbox. Given the rotational frequency f_a of the rotor hub, the rotational frequency of sun shaft is computed from the following equation

$$f_s = f_a \cdot r_{PS} \quad (5)$$

The mesh frequency of the PS is shown as.

$$f_{PS} = f_a \cdot Z_r = (f_s - f_a) \cdot Z_s \quad (6)$$

The mesh frequency of the IS is expressed as.

$$f_{IS} = f_s \cdot Z_{mi} \quad (7)$$

The rotational frequency of the intermediate shaft is shown as.

$$f_i = f_s \cdot r_{IS} \quad (8)$$

The mesh frequency of the HSS is expressed as.

$$f_{HSS} = f_i \cdot Z_{hi} \quad (9)$$

Expression (10) presents the rotational frequency of the high speed shaft.

$$f_h = f_i \cdot r_{HSS} \quad (10)$$

Similarly, knowing the rotational frequency of the high speed shaft, the mesh and rotational frequencies of other shafts can be derived.

3 Fault detection in the wind turbine gearbox

3.1 Multi-scale enveloping spectrogram

Continuous wavelet transform (CWT) is used for processing non-stationary signals. Signal $x(t)$ is decomposed into different time-frequency grids by adjusting scale factor a and time factor τ as shown as.

$$wt(a, \tau) = |a|^{-1/2} \int_{-\infty}^{\infty} x(t) \varphi^* \left(\frac{t-\tau}{a} \right) dt \quad (11)$$

where $\varphi(t)$ is a wavelet function represented as, for example, the Morlet wavelet, harmonic wavelet, or the Mexican hat wavelet.

Although CWT offers multi-scale decomposition of the vibration signal, it is unable to directly extract modulation components that may indicate a fault. The authors in [22, 23] researched the complex wavelet transform and they proposed MuSEnS.

A complex wavelet [22, 23] is defined in the following equation.

$$\varphi(t) = \varphi_R(t) + j\varphi_I(t) = \varphi_R(t) + jH[\varphi_R(t)] \quad (12)$$

where, $\varphi_R(t)$ is the real part of the complex wavelet, $\varphi_I(t)$ is the imaginary part of the complex wavelet, and $\varphi_I(t)$ is the Hilbert transform of $\varphi_R(t)$. For example, the Gaussian wavelet used in this paper is expressed as.

$$\varphi_G(t) = C_N \frac{d^{(N)}(e^{-j^t} e^{-t^2})}{dt^N} \quad (13)$$

where, $d^{(N)}/dt^N$ is the N th order derivative and C_N is a constant related to the order. Fig. 2 shows the fourth order complex Gaussian wavelet.

The complex wavelet transform of $x(t)$ is expressed as.

$$wt_C(a, \tau) = wt_R(a, \tau) + j wt_I(a, \tau) \quad (14)$$

where

$$\begin{cases} wt_R(a, \tau) = |a|^{-1/2} \int_{-\infty}^{\infty} x(t) \varphi_R^* \left(\frac{t-\tau}{a} \right) dt \\ wt_I(a, \tau) = |a|^{-1/2} \int_{-\infty}^{\infty} x(t) H \left[\varphi_R^* \left(\frac{t-\tau}{a} \right) \right] dt \end{cases} \quad (15)$$

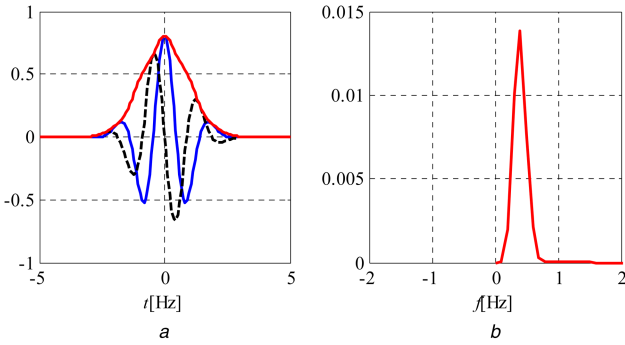


Fig. 2 Complex Gaussian wavelet
 (a) Real part of the complex wavelet (shown in blue), imaginary part of the complex wavelet (black and dashed), modulus of the complex wavelet (red), (b) FFT of the modulus of the complex wavelet

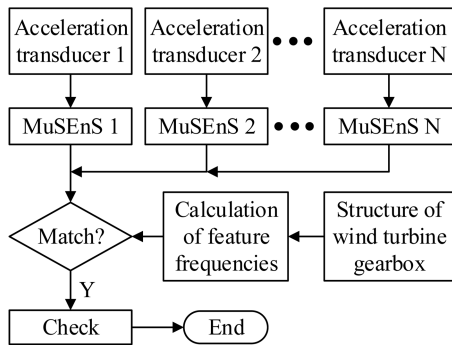


Fig. 3 Fault diagnosis procedure for wind turbine gearbox

From the modulus of the $w_{tC}(a, \tau)$ in (14), the envelope signal in (16) is generated.

$$e_{wt}(a, \tau) = \frac{\| w_{tC}(a, \tau) \|}{\sqrt{w_{tR}(a, \tau)^2 + H[w_{tR}(a, \tau)]^2}} \quad (16)$$

Furthermore, based on the Fourier transform, MuSEnS in (17) is computed.

$$E_{wt}(a, f) = F(\| w_{tC}(a, \tau) \|) = \frac{1}{2\pi} \int_{-\infty}^{\infty} \| w_{tC}(a, \tau) \| e^{-j2\pi f \tau} d\tau \quad (17)$$

The expression (16) is similar to the envelope signal of the Hilbert demodulation analysis [24]. MuSEnS inherits the property of

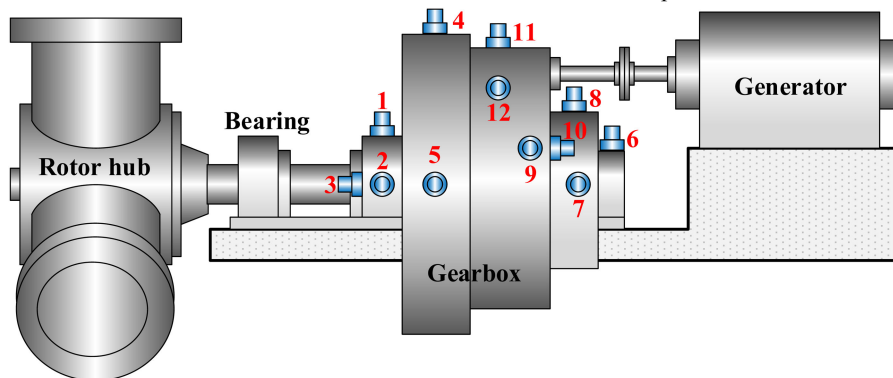


Fig. 4 Placement of the acceleration transducers on gearbox

Table 1 Numbers of teeth of multiple gears in wind turbine gearbox

Z_p	Z_s	Z_r	Z_{mi}	Z_{mo}	Z_{hi}	Z_{ho}
35	17	87	101	24	82	21

multi-scale decomposition of CWT that does not select a narrow band to filter the original vibration signal. Thus, it enables filtering signals at different bandwidth and generating demodulation information.

3.2 Fault diagnosis procedure

The gears and bearings installed in a wind turbine gearbox may generate different fault feature frequencies. The frequency may span from about 0.2 Hz (rotational frequency of the rotor) to hundreds of Hz (mesh frequency of the HSS). This calls for the capability to handle a wide range of frequencies.

Acceleration transducers with different sensitivity are installed on the surface of the gearbox to acquire vibration signals. Each of transducer is responsible for a segment of the gearbox. The diagnosis procedure of the wind turbine gearbox is shown in Fig. 3.

As illustrated in Fig. 3, the multi-channel vibration signals from different segments of the gearbox are collected, and the corresponding MuSEnSs are obtained. The feature frequencies of gears or bearings in gearbox are computed according to gearbox structure in Fig. 1. If the evident harmonic components of the MuSEnS are matched with the computed feature frequencies, we can conclude the potential faults and check for the wind turbine gearbox using endoscope or other equipment.

4 Case study

4.1 Wind turbine considered in this research

The wind turbine used in this research has a rated power of 2.0 MW. To find potential faults in the gearbox, 12 different segments of the gearbox were tested. The gearbox in Fig. 4 is instrumented with 12 transducers. The transducers 1–3 are used to monitor the condition of rear main bearing, transducers 4 and 5 are responsible for PS, transducers 6–10 are used to monitor the gears and bearings in IS, transducers 11 and 12 are for HSS. Since the rotational speed of PS is low, the sampling frequency of first five channels is 5120 Hz, while the one of the last seven channels is 25,600 Hz.

The numbers of teeth of multiple gears in the gearbox is shown as in Table 1. The transmission ratio of PS is 6.12, the IS is 4.21 and HSS is 3.9. The total transmission ratio of the gearbox is 100.53. The rated rotational speed of the generator is 1678.85 rpm/min. However, the measured rotational speed of the generator is not always identical to the rated value due to varying wind speed. Table 2 list the rotational shaft and gear mesh frequencies during one test when rotational frequency of generator is 23.6 Hz.

4.2 Analysis for the results

The acquired 12-channel vibration signals are shown as in Fig. 5. The vibration amplitude does not exceed $\pm 30 \text{ m/s}^2$, even for the

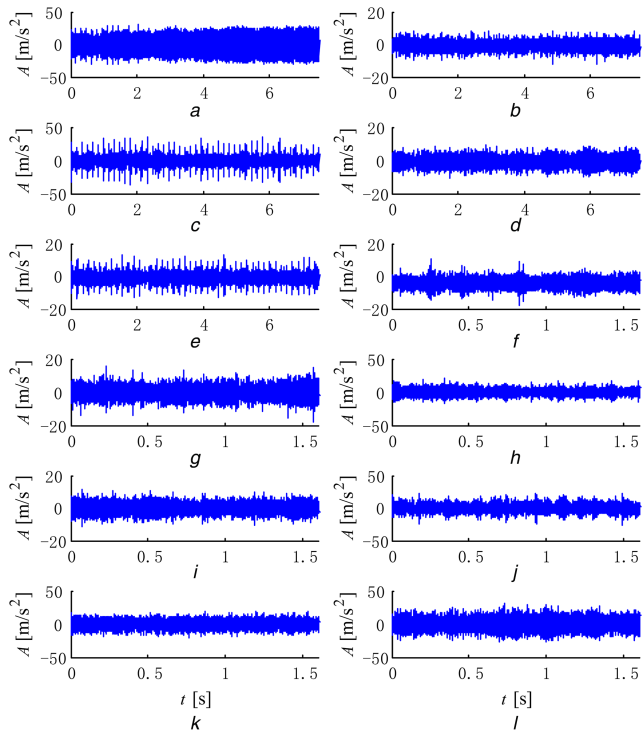


Fig. 5 Vibration signals from 12 different segments of gearbox

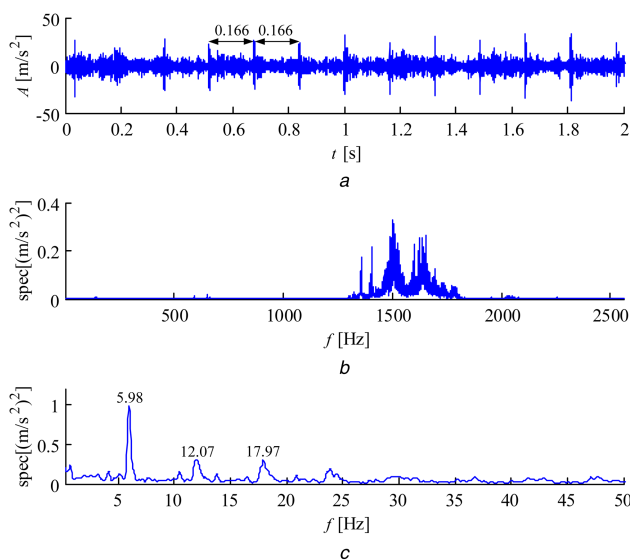


Fig. 6 Power spectrum and envelope spectrum (a) Time signal of transducer 3, (b) Power spectrum, (c) Envelope spectrum after bandpass filtering from 1300 Hz to 1800 Hz

transducers 11 and 12 located in the neighbourhood of the high speed stage. It is difficult to determine whether fault is reflected in the vibration amplitude. There are obvious periodic impacts in Figs. 5c and e, which indicate possible fault in gearbox. The interval of impacts is about 0.167 s that approaches the rotational frequency f_i of intermediate shaft in Table 2. It is easily deduced that one of the two gears on intermediate shaft may be damaged.

Figs. 6 and 7 are the power spectra and envelope spectra of vibration signals from transducers 3 and 5. In Fig. 6b, the vibration energy concentrates between 1300 and 1800 Hz that may be certain natural frequency of gear or gearbox. The impact 5.98 Hz and its harmonics are demodulated in Fig. 6c. In Fig. 7b, the vibration

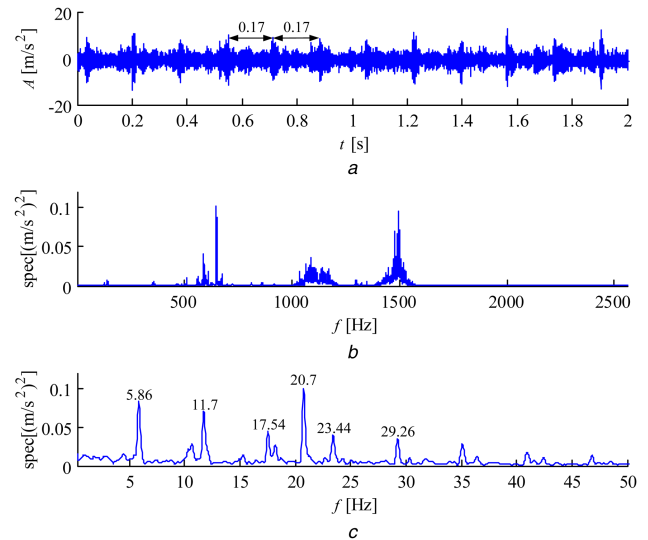


Fig. 7 Power spectrum and envelope spectrum (a) Time signal of transducer 5, (b) Power spectrum, (c) Envelope spectrum after bandpass filtering from 1350 Hz to 1600 Hz

energy disperses into three different frequency bands that cannot accord with any mesh frequency. However still in Fig. 7c, the rotational frequencies of intermediate shaft are obvious. Besides of these, the mesh frequency 20.7 Hz of PS arises.

To detect and diagnose faults in the wind turbine gearbox, MuSenS is applied to analyse all the 12-channel vibration signals. The MuSenSs are shown as in Fig. 8. Scanning from Figs. 8a–l, the rotational frequency of intermediate shaft and its harmonics appear in all the figures. The frequencies of intermediate shaft in Fig. 8 are different because the channels are tested one by one at different times when wind speed and rotational speed of rotor are varying.

In addition, there are evident rotational frequency about 21 Hz of high speed shaft and its two order harmonic in Figs. 8f, i and j, which may indicate fault on gear of high speed shaft. Fig. 9 are the slices of MuSenS in Fig. 8f at scale 10 and 25, respectively, and 21.67, 43.75 Hz are distinct in Fig. 9b. It is also worth noting that low-frequency components are highlighted in Figs. 8h and k, circled by red ellipses. Fig. 10 are the slices of Fig. 8k at scale 40 and 22 where the frequencies 1.458 and 2.917 Hz are towering. The distinct components in Fig. 10b agree with the rotational frequency of sun shaft in Table 2. Thus, we infer that there may be fault on the big gear on the sun shaft.

4.3 Validation for the vibration analysis

From the analysis in Section 4.2, three rotational frequencies are obtained when observing the MuSenSs. The most notable one is the rotational frequency of intermediate shaft that indicates gear failure on this shaft. It is not difficult to find the rotational frequency of high speed shaft in Fig. 8f, i and j, which may denote gear fault on high speed shaft. Since the high-speed shaft is connected with generator through coupling, it is easy to be imbalance or misalignment that can also generate the component of rotational frequency. Therefore, the rotational frequency of high speed shaft does not necessarily reflect gear fault. A weak fault feature that is easily neglected but very significant is the rotational frequency of sun shaft. Although there are two gears installing on this shaft, only the big gear rather than sun gear should be represented by the rotational frequency. The fault feature of sun gear is denoted by the difference between rotational frequency of sun shaft and planetary arm [18].

Table 2 Shaft rotational frequencies and gear meshing frequencies

f_r	f_s	f_i	f_h	f_{PS}	f_{IS}	f_{HSS}
0.234	1.43	6.04	23.6	20.4	144.9	495.3

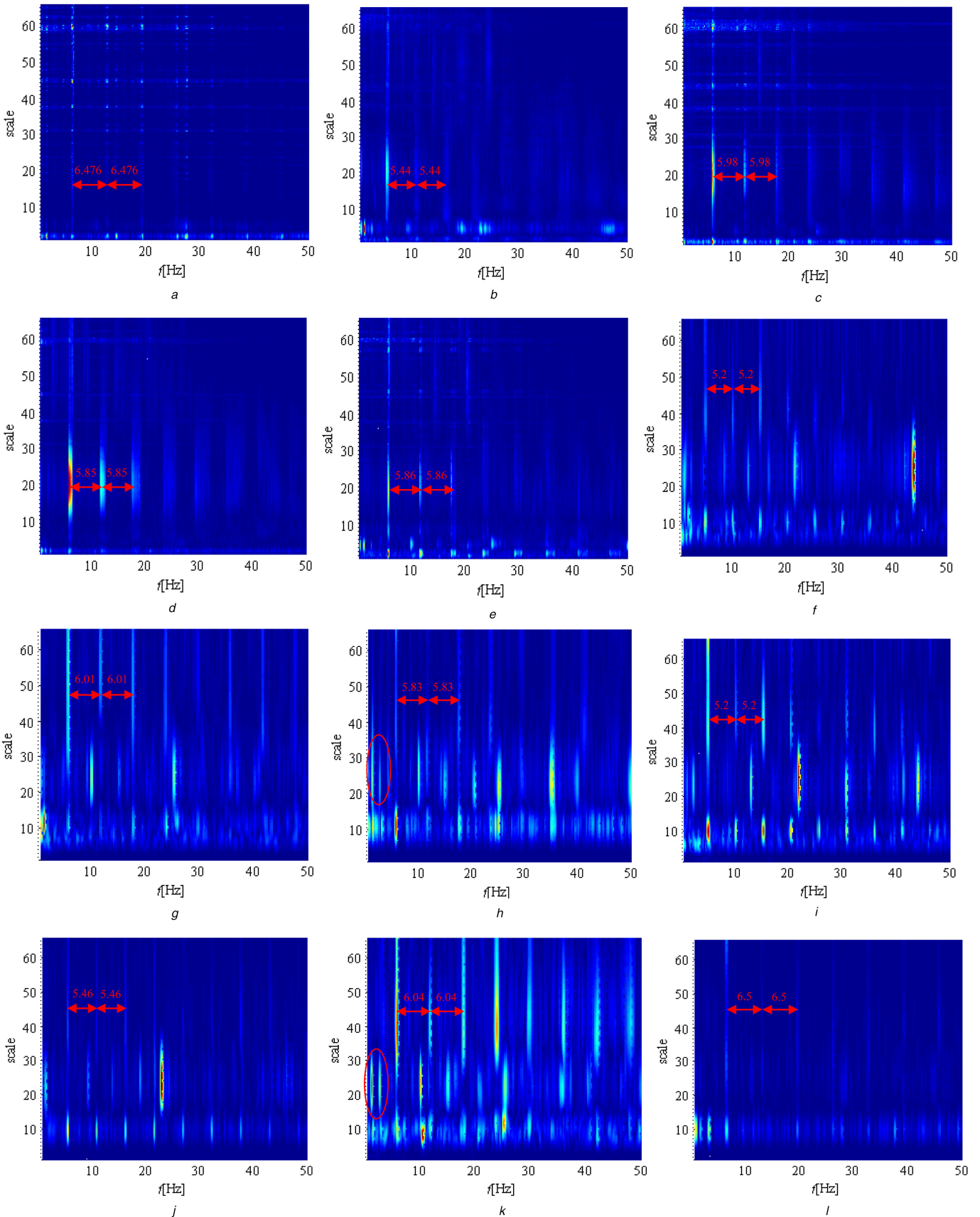


Fig. 8 MuEnSs of vibration signals from 12 different segments of gear box

The disassembled results verify the diagnosis conclusion above. Fig. 11 shows the serious broken gear on intermediate shaft in IS. Such a severe fault excites the obvious rotational frequency in all vibration channels. Observing Fig. 12 the gear on high speed shaft, there is only renewable scratch on it, which does not tally with the evident rotational frequency of high speed shaft. Thus the

rotational frequency of high speed shaft may be caused by imbalance or misalignment. Little crack is found on the big gear of sun shaft, shown as in Fig. 13, which is corresponding to the rotational frequency of sun shaft analysed in Figs. 8k and 10b.

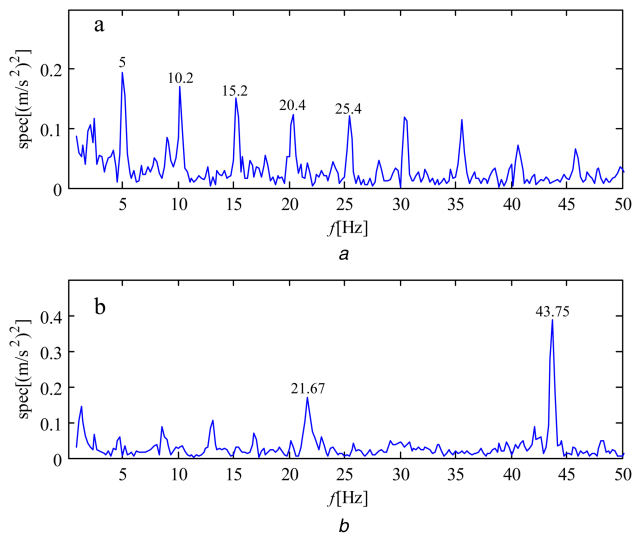


Fig. 9 Slices of MuSenS in Fig. 8f
(a) At scale = 10, (b) At scale = 25

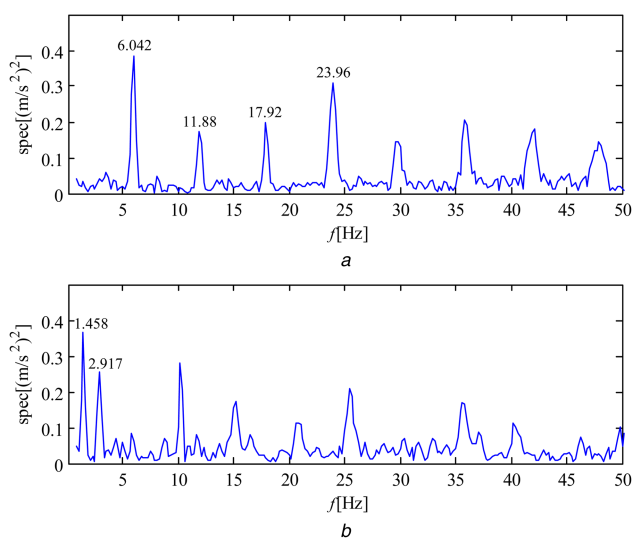


Fig. 10 Slices of MuSenS in Fig. 8k
(a) At scale = 40, (b) At scale = 22



Fig. 11 Broken gear on intermediate shaft in IS

5 Conclusion

MuSenS can decompose vibration signal into different frequency bands due to the multi-scale characteristic, and simultaneously obtain corresponding envelope spectrum that represents modulation information in wind turbine gearbox.

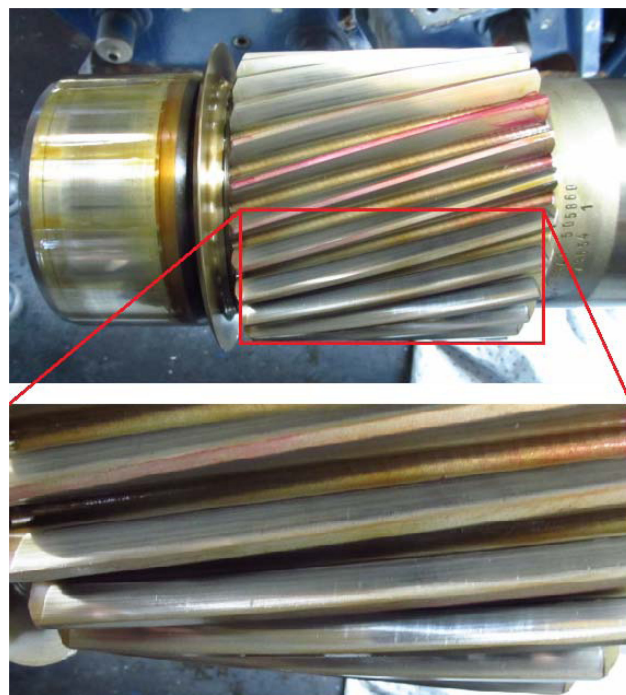


Fig. 12 Gear on high speed shaft



Fig. 13 Cracked big gear on sun shaft in IS

In this paper, a MuSenS based fault diagnosis procedure is proposed to analyse and process the vibration signals from a real 2.0 MW wind turbine gearbox. Not only the evident fault feature denoting gear fault on intermediate shaft can be found, but the weak fault of big gear on sun shaft is detected distinctly. The disassembled gears demonstrate the effectiveness of diagnosis results. The MuSenS-based method is a practical diagnosis tool for real wind turbine.

6 Acknowledgments

The research presented in this paper was supported by National Natural Science Foundation of China (grant no. 51305135), Science and Technology Plan Projects of Hebei (grant no. 15214307D), the Fundamental Research Funds for the Central Universities of China (grant no. 2015ZD15), and the National High Technology Research and Development Program of China (863 Program) (grant no. 2015AA043702).

7 References

- [1] Becker, E., Poste, P.: 'Keeping the blades turning: condition monitoring of wind turbine gears', *Refocus*, 2006, 7, (2), pp. 26–32

- [2] Ribrant, J., Bertling, L.M.: 'Survey of failures in wind power systems with focus on Swedish wind power plants during 1997-2005', *IEEE Trans. Energy Convers.*, 2007, **22**, (1), pp. 167-173
- [3] Wiggelinkhuizen, E., Verbruggen, T., Braam, H., *et al.*: 'Assessment of condition monitoring techniques for offshore wind farms', *J. Solar Energy Eng.*, 2008, **130**, (3), pp. 031004-1-9
- [4] Salem, A.A., Abu-Siada, A., Islam, S.: 'Condition monitoring techniques of the wind turbines gearbox and rotor', *Int. J. Electr. Energy*, 2014, **2**, (1), pp. 53-56
- [5] Amirata, Y., Benbouzida, M.E.H., Al-Ahmara, E., *et al.*: 'A brief status on condition monitoring and fault diagnosis in wind energy conversion systems', *Renew. Sustain. Energy Rev.*, 2009, **13**, (9), pp. 2629-2636
- [6] Wymore, M.L., Dam, J.E.V., Ceylan, H., *et al.*: 'A survey of health monitoring systems for wind turbines', *Renew. Sustain. Energy Rev.*, 2015, **52**, pp. 976-990
- [7] Tchakoua, P., Wamkeue, R., Ouhrouche, M., *et al.*: 'Wind turbine condition monitoring: state-of-the-art review, new trends, and future challenges', *Energies*, 2014, **7**, pp. 2595-2630
- [8] Yang, W., Tavner, P.J., Wilkinson, M.R.: 'Condition monitoring and fault diagnosis of a wind turbine synchronous generator drive train', *IET Renew. Power Gener.*, 2009, **3**, (1), pp. 1-11
- [9] Zhang, Z., Verma, A., Kusiak, A.: 'Fault analysis and condition monitoring of the wind turbine gearbox', *IEEE Trans. Energy Convers.*, 2012, **27**, (2), pp. 526-535
- [10] Feng, Z.P., Zuo, M.J.: 'Fault diagnosis of planetary gearboxes via torsional vibration signal analysis', *Mech. Syst. Signal Process.*, 2013, **36**, (2), pp. 401-421
- [11] Lapira, E., Brisset, D., Ardakani, H.D., *et al.*: 'Wind turbine performance assessment using multi-regime modeling approach', *Renew. Energy*, 2012, **45**, pp. 86-95
- [12] Herp, J., Pedersen, N.L., Nadimi, E.S.: 'Wind turbine performance analysis based on multivariate higher order moments and Bayesian classifiers', *Control Eng. Pract.*, 2016, **49**, pp. 204-211
- [13] Lei, Y.G., Han, D., Lin, J., *et al.*: 'Planetary gearbox fault diagnosis using an adaptive stochastic resonance method', *Mech. Syst. Signal Process.*, 2013, **38**, (1), pp. 113-124
- [14] Li, J.M., Chen, X.F., Du, Z.H., *et al.*: 'A new noise-controlled second-order enhanced stochastic resonance method with its application in wind turbine drivetrain fault diagnosis', *Renew. Energy*, 2013, **60**, (4), pp. 7-19
- [15] Teng, W., Wang, F., Zhang, K.L., *et al.*: 'Pitting fault detection of a wind turbine gearbox using empirical mode decomposition', *Strojnicki vestnik - J. Mech. Eng.*, 2014, **60**, (1), pp. 12-20
- [16] Sun, H., Zi, Y., He, Z.: 'Wind turbine fault detection using multiwavelet denoising with the data-driven block threshold', *Appl. Acoust.*, 2014, **77**, pp. 122-129
- [17] Barszcz, T., Randall, R.B.: 'Application of spectral kurtosis for detection of a tooth crack in the planetary gear of a wind turbine', *Mech. Syst. Signal Process.*, 2009, **23**, (4), pp. 1352-1365
- [18] Feng, Z.P., Zuo, M.J.: 'Vibration signal models for fault diagnosis of planetary gearboxes', *J. Sound Vib.*, 2012, **331**, (22), pp. 4919-4939
- [19] Feng, Z.P., Liang, M., Zhang, Y., *et al.*: 'Fault diagnosis for wind turbine planetary gearboxes via demodulation analysis based on ensemble empirical mode decomposition and energy separation', *Renew. Energy*, 2012, **47**, (1), pp. 112-126
- [20] Feng, Z.P., Chen, X., Liang, M.: 'Iterative generalized synchrosqueezing transform for fault diagnosis of wind turbine planetary gearbox under nonstationary conditions', *Mech. Syst. Signal Process.*, 2015, **52-53**, pp. 360-375
- [21] Feng, Z.P., Liang, M.: 'Fault diagnosis of wind turbine planetary gearbox under nonstationary conditions via adaptive optimal kernel time-frequency analysis', *Renew. Energy*, 2014, **66**, pp. 468-477
- [22] Yan, R.Q., Gao, R.X.: 'Multi-scale enveloping spectrogram for vibration analysis in bearing defect diagnosis', *Tribol. Int.*, 2009, **42**, (2), pp. 293-302
- [23] Wang, J.J., Gao, R.X., Yan, R.Q.: 'Multi-scale enveloping order spectrogram for rotating machine health diagnosis', *Mech. Syst. Signal Process.*, 2014, **46**, (1), pp. 28-44
- [24] Feldman, M.: 'Hilbert transform in vibration analysis', *Mech. Syst. Signal Process.*, 2011, **25**, (3), pp. 735-802